Monitoring Tumor Glucose Utilization by Positron Emission Tomography for the Prediction of Treatment Response to Epidermal Growth Factor Receptor Kinase Inhibitors

Helen Su,[1,4] Claudia Bodenstein,[1,4] Rebecca A. Dumont,[1,4] Yann Seimbille,[1] Steven Dubinett,[2] Michael E. Phelps,[1] Harvey Herschman,[1,2,3] Johannes Czernin,[1,4] and Wolfgang Weber[1,4]

Abstract

Purpose: The mechanisms underlying the sensitivity of non – small cell lung cancer to epidermal growth factor receptor (EGFR) kinase inhibitors are complex, and there are no established markers to accurately predict treatment outcome in individual patients.

Experimental Design: We investigated whether tumors responding to EGFR inhibitors can be identified by measuring treatment-induced changes in glucose utilization by positron emission tomography with the glucose analogue fluorodeoxyglucose (FDG-PET). We studied a panel of cell lines with a spectrum of sensitivity to EGFR kinase inhibitors. After incubation with the EGFR kinase inhibitor gefitinib for various time points, FDG uptake, glucose transport rates, and hexokinase activity were determined. FDG uptake *in vivo* was assessed by microPET imaging of tumor xenografts in mice.

Results: In gefitinib-sensitive cell lines, there was a dramatic decrease in FDG uptake as early as 2 hours after treatment. Immunoblots showed the translocation of glucose transporters (GLUT3) from the plasma membrane to the cytosol; glucose transport rates were reduced 2.6-fold at this time. There was also a modest reduction of hexokinase activity. These metabolic alterations preceded changes in cell cycle distribution, thymidine uptake, and apoptosis. MicroPET studies showed an up to 55% decrease of tumor FDG uptake in sensitive xenografts within 48 hours. In contrast, gefitinib-resistant cells exhibited no measurable changes in FDG uptake, either in cell culture or *in vivo*.

Conclusion: Glucose metabolic activity closely reflects response to gefitinib therapy. FDG-PET may be a valuable clinical predictor, early in the course of treatment, for therapeutic responses to EGFR kinase inhibitors.

Two small molecule inhibitors of the epidermal growth factor receptor (EGFR) tyrosine kinase (gefitinib and erlotinib), have recently been approved (1–3) for the treatment of advanced, chemotherapy-refractory, non–small cell lung cancers (NSCLC). Both drugs can induce dramatic clinical responses, but only in small subgroups of patients. For the majority of patients with NSCLC, the beneficial effects of treatment with EGFR kinase inhibitors seem to be limited. Therefore, patient selection is critical for the clinical use of approved EGFR kinase inhibitors, as well as for future clinical trials, in this disease.

Several clinical and histologic characteristics have been shown to correlate with responsiveness to EGFR kinase inhibitors (4, 5). Recently, specific mutations of the EGFR kinase domain have been identified to confer sensitivity to gefitinib and erlotinib (6–8). Although this observation provides highly valuable insights into the molecular mechanisms underlying sensitivity to EGFR kinase inhibitors, none of the known clinical or molecular tumor characteristics allows the accurate prediction of tumor response in an individual patient (4, 5). Therefore, there is a clear need for new approaches to identify patients who will benefit from treatment with EGFR kinase inhibitors.

In this study, we evaluated whether the assessment of tumor glucose utilization by positron emission tomography (PET) with the glucose analogue, fluorodeoxyglucose (FDG), could be used to predict tumor response to EGFR kinase inhibitors early in the course of therapy. Previous studies have suggested that changes in tumor FDG uptake provide an early readout for the efficacy of conventional chemotherapy in NSCLC and in other tumor types (9–11). Furthermore, dramatic changes in tumor FDG uptake have been observed in patients with gastrointestinal stromal tumors treated with imatinib, a tyrosine kinase inhibitor with distinct target specificity (12, 13). Based on these

Authors' Affiliations: [1]Department of Molecular Medicine and Pharmacology, [2]Jonsson Comprehensive Cancer Center, [3]Department of Biological Chemistry, and [4]Ahmanson Biological Imaging Center, David Geffen School of Medicine, University of California at Los Angeles, Los Angeles, California

Received 2/15/06; revised 3/31/06; accepted 4/20/06.

Grant support: UCLA Center for *In Vivo* Imaging in Cancer Biology (NIH P50 CA86306), UCLA Institute of Molecular Medicine (DE-FC03-87E60615), and UCLA Lung Specialized Programs of Research Excellence (NIH P50 CA9038).

The costs of publication of this article were defrayed in part by the payment of page charges. This article must therefore be hereby marked *advertisement* in accordance with 18 U.S.C. Section 1734 solely to indicate this fact.

Requests for reprints: Wolfgang Weber, Department of Molecular Medicine and Pharmacology, David Geffen School of Medicine, University of California at Los Angeles, CHS AR-274, 650 Charles Young Drive, South Los Angeles, CA 90095. Phone: 310-206-2179; Fax: 310-206-4899; E-mail: wweber@mednet.ucla.edu.

doi:10.1158/1078-0432.CCR-06-0368

precedents, we hypothesized that similar changes in glucose metabolism may also occur, and may be useful in monitoring the response to targeted therapy in NSCLC tumors that are sensitive to EGFR kinase inhibitors.

Materials and Methods

Cell cultures. We used four NSCLC cell lines (A549, H3255, HCC4006, and H1975) and an epithelial carcinoma cell line with EGFR amplification (A431). A431, A549, and H1975 were obtained from the American Tissue Culture Collection (Rockville, MD). H3255 and HCC4006 were kindly provided by Dr. Bruce Johnson (Dana-Farber Cancer Institute, Boston, MA) and Dr. John Minna (the University of Texas Southwestern, Dallas, TX), respectively. The EGFR status of these cells, described in previous studies (6, 14–17), is summarized in Table 1. All cells were grown in RPMI 1640 (Invitrogen, Carlsbad, CA) supplemented with 10% fetal bovine serum (Omega Scientific, Tarzana, CA), 2 mg/mL glucose, 100 units/mL of penicillin, and 100 units/mL of streptomycin (Invitrogen). Cells were grown at 37°C in an atmosphere of 5% CO_2.

Growth curve analysis. Cells were plated in six-well plates (Costar, Cambridge, MA) at 0.5 to 1×10^5 cells per well. After 24 hours, various amounts of gefitinib were added into each well. Gefitinib was synthesized in our lab according to published procedures (18), and dissolved in DMSO. Quality control of gefitinib was done by nuclear magnetic resonance, high-resolution mass spectrometer, and reversed phase high-pressure liquid chromatography, as reported previously (18). The chemical purity was >98%. Viable cell numbers from triplicate wells were determined every 24 hours for 4 days by trypan blue exclusion using the Vi-Cell XR instrument (Beckman Coulter, Fullerton, CA).

Western blot analysis. Following treatment with gefitinib, protein expression and phosphorylation status were assessed by Western blotting of cell lysates. When indicated, cells were stimulated with 100 ng/mL of epidermal growth factor for 15 minutes prior to preparation of the lysates as described previously (19). Antibodies used for Western blotting included anti-phospho-EGFR (Y1173) mouse monoclonal antibody, clone 9H2 (Upstate, Lake Placid, NY); anti-actin mouse monoclonal antibody (Sigma, St. Louis, MO); rabbit anti-VDAC1 antibody (Abcam, Cambridge, MA); sheep anti-GLUT1 and anti-GLUT3 antibodies (Abcam, Cambridge, MA); anti-Na, K-ATPase mouse antibody (Abcam, Cambridge, MA); mouse anti-AKT (2H10) monoclonal antibody and mouse anti-phospho-AKT (Ser^{473}; 587F11) monoclonal antibody (Cell Signaling, Beverly, MA). Peroxidase-conjugated goat anti-mouse IgG and peroxidase-conjugated goat anti-rabbit IgG (both from Jackson ImmunoResearch, West Grove, PA) were used as the secondary antibodies for the Western blots. All blots were done according to the manufacturer's instructions.

Table 1. EGFR status and gefitinib sensitivity of the cell lines used in this study

Cell line	Gefitinib IC_{50} (μmol/L)	EGFR status
A431	0.2	Wild-type, amplification (14, 15)
A549	11.9	Wild-type (15)
H1975	7.1	L858R, T790M (16)
H3255	<0.2	L858R (6)
HCC4006	<0.2	Exon 19 deletion (17)

NOTE: IC_{50} values were calculated from growth curve assays done on cell lines treated for 4 days with various concentrations of gefitinib.

Radioactive glucose and thymidine analogues. Synthesis and quality control of [^{18}F]fluorodeoxyglucose (FDG) and [^{18}F]fluorothymidine (FLT) were done by the UCLA Cyclotron Facility, as previously described (20). For both FDG and FLT, the radiochemical purities were >99%, and the specific activities were >1,000 Ci/mmol. 3-*O*-[methyl-^{3}H] Glucose (3-OMeG; specific activity, 60 Ci/mmol) was obtained from Moravek Biochemicals (Brea, CA).

Cellular uptake of FDG and FLT. Cells were plated in six-well plates (Costar) at 1×10^5 cells per well 1 day prior to the uptake experiment. On the day of the experiment, uptake medium containing FDG or FLT at 1 μCi/mL was added to each well. Glucose-free medium was used for FDG uptake. All uptake studies were done for 60 minutes at 37°C. Preliminary studies indicated that FDG and FLT uptake is linear over this period of time for all cell lines, and that there is no depletion of the radioactive substrates from the culture media. Triplicate wells were then rinsed twice in cold PBS, harvested with trypsin to determine cell-associated fluorine-18 radioactivity, using a Packard 5600 gamma counter (Packard, Meriden, CT). Washing did not induce significant efflux of FDG, as confirmed by preliminary studies comparing FDG uptake of cells washed for different periods of time in the presence or absence of the glucose transport inhibitors, cytochalasin B and phloretin. This indicates that after an incubation period of 60 minutes, almost all FDG was trapped intracellularly as FDG-6-phosphate. Radioactivity uptake values were normalized to the number of viable (trypan blue–negative) cells, and expressed relative to untreated controls.

Cell cycle and apoptosis analysis. After being treated with gefitinib in the same way as described for the cell uptake studies, cells were stained with propidium iodide (Calbiochem, San Diego, CA) and RNase A (Sigma, MO) in a hypotonic buffer. The DNA content was then analyzed by a FACScan flow cytometer (Becton Dickinson, Franklin Lakes, NJ) using the CellQuest 3.1 software (Becton Dickinson) for acquisition, and the ModFit LT 2.0 software (Verity, Topsham, ME) for analysis. For assessment of cellular apoptosis, cells were stained with FITC-conjugated Annexin V from the Apoptosis Detection Kit II (BD Biosciences, San Jose, CA), and analyzed with FACScan (Becton Dickinson), gating out doublets and clumps using pulse processing, and collecting fluorescence above 620 nm.

Cellular fractionation. Mitochondrial fractionation was done using a mitochondria isolation kit from Pierce (Rockford, IL). Plasma membrane fractionation was done using the plasma membrane protein extraction kit from Biovision (Mountain View, CA). Fraction purity was assessed by Western blot analysis of the mitochondrial marker, VDAC/Porin (21); and the plasma membrane marker, Na^+, K^+-ATPase (22), respectively.

Hexokinase assay. Cells were harvested, washed twice in cold PBS, and lysed in extraction buffer [45 mmol/L Tris-HCl (pH 8.2), 50 mmol/L KH_2PO_4, 10 mmol/L glucose, 11.1 mmol/L monothioglycerol, 0.5 mmol/L EDTA, 0.2% Triton X-100]. Mitochondrial fractions were also resuspended in this extraction buffer. Extracts were assayed for hexokinase activity by a standard G-6-P dehydrogenase-coupled spectrophotometric assay (23), in a final solution containing 50 mmol/L of Tris-HCl (pH 8), 1 mol/L of glucose, 6.8 mol/L of NAD, 100 mmol/L of ATP, 13.3 mmol/L of $MgCl_2$, 30 units of G6DPH, and the cellular extracts. The reaction was started by the addition of extract samples and monitored at 340 nm at room temperature using the UV-Visible Spectrophotometer 8453 (Agilent Technologies, Palo Alto, CA).

Measurement of glucose transport by 3-OMeG. Cells were plated in six-well plates (Costar) at 1×10^5 cells per well 1 day prior to the uptake experiment. On the day of the experiment, cells were incubated with 3-OMeG (1 μCi/mL) and cold 3-OMeG from 10 seconds to 3 minutes at a final concentration of 0.05 mmol/L 3-OMeG, as previously described (24). Triplicate wells were washed with ice-cold PBS supplemented with 100 mmol/L of phloretin, and lysed with 0.1% SDS. The cell lysates were collected, scintillation fluid (ICN, Costa Mesa, CA) was added, and ^{3}H radioactivity was determined quantitatively in a Packard β-counter calibrated with quenched ^{3}H standards.

Time activity curves for cellular uptake of 3-OMeG (normalized as described for the FDG uptake studies) were fitted by using GraphPad Prism 4.0 (GraphPad Software, San Diego, CA) and initial transport rates as well as uptake at equilibrium were calculated.

Xenograft model. Severe combined immunodeficient (*Scid/Scid*) mice were purchased from The Jackson Laboratory (Bar Harbor, MN). All animal manipulations were done with sterile techniques following the guidelines of the UCLA Animal Research Committee. Cells (1-2 $\times$ 10^6 cells per mouse) growing exponentially in culture were removed from the plate with trypsin, resuspended in PBS and Matrigel (BD Biosciences, Bedford, MA), and injected s.c. into the right hind leg or flank of severe combined immunodeficient mice. Animals underwent a first microPET/CT scan after tumors had grown to an approximate size of 100 mm^3. Groups of at least three mice were then randomized for treatment with 70 mg/kg/d of gefitinib versus vehicle. All mice underwent a second microPET/CT scan 2 days later.

MicroPET and microCT imaging. MicroPET/CT scans were done using the microPET FOCUS 220 PET scanner (ref. 25; Siemens Preclinical Solutions, Knoxville, TN) and MicroCAT II CT scanner (Siemens Preclinical Solutions). Mice were fasted for 6 hours prior to FDG injection and placed on a heating pad (30°C) starting 30 minutes prior to FDG injection. For FDG injection and imaging, mice were anesthetized using 1.5% to 2% isoflurane. Mice were imaged in a chamber that minimizes positioning errors between PET and CT to <1 mm (26). Imaging was started 60 minutes after an i.p. injection of 200 to 300 μCi of FDG. Image acquisition time was 10 minutes. Immediately after the PET scan, the mice underwent a 7-minute microCT scan, using routine image acquisition variables (26). Images were reconstructed by filtered back-projection, using a ramp filter with a cutoff frequency of 0.5 Nyquist. Image counts per pixel per second were calibrated to activity concentrations (Bq/mL) by measuring a 3.5-cm cylinder phantom filled with a known concentration of FDG. For display, activity concentrations were expressed as a percentage of the decay-corrected injected activity per gram of tissue by using AMIDE software (27). Spherical regions of interests (2 mm diameter) were placed in the area of the tumor with the highest FDG uptake. To account for interindividual differences in FDG biodistribution, a spherical region of interest with a diameter of 4 mm was placed in the liver as a reference region (28). Tumor FDG uptake was then expressed as the ratio between the mean activity concentrations in the tumor divided by the mean activity concentration in the liver. Gefitinib treatment did not induce systematic changes in liver FDG uptake. Regions of interest were defined in the PET/CT fusion images generated by the AMIDE software to ensure accurate anatomic positioning of the regions of interest in the tumor and liver.

Statistical analysis. Quantitative results are expressed as mean $\pm$ 1 SE. Comparisons were made by *t* tests as well as by ANOVA as appropriate. Significant associations in ANOVA were further analyzed by Bonferroni *post hoc* tests. Differences were considered significant when $P < 0.05$.

Results

Sensitivity of cells to gefitinib. We first selected H3255 and A549 cells as models for gefitinib-sensitive and gefitinib-resistant cells. As reported previously, H3255 cells were highly sensitive to gefitinib, cell growth was significantly inhibited at a concentration of 0.2 μmol/L ($P < 0.01$, Fig. 1A). This growth-inhibitory effect of gefitinib was paralleled by an inhibition of EGFR and AKT phosphorylation (Fig. 1B). In contrast, the growth of A549 cells was only inhibited at a concentration of 20 μmol/L of gefitinib. Even at this high concentration, there was no measurable decrease in Akt phosphorylation (Fig. 1A and B).

Uptake of FDG reflects immediate cellular response to gefitinib treatment. In H3255 cells, FDG uptake per viable cell was reduced to <50% of vehicle controls within 2 hours of gefitinib therapy ($P < 0.01$, Fig. 1C). In contrast, gefitinib did not significantly affect the cellular uptake levels of FDG in the gefitinib-resistant A549 cells, regardless of treatment time or dose ($P > 0.08$, Fig. 1C).

Changes in FDG uptake precede inhibition of cellular proliferation and induction of apoptosis by gefitinib. Four hours after incubation with 0.2 μmol/L of gefitinib, there were no differences in cell cycle distribution for treated H3255 cells and controls (Fig. 2A). However, at day 2 of gefitinib treatment, 90% of the cell population was arrested in G_1. No significant difference in cell cycle patterns were observed in A549 cells at all time points (data not shown). As a second measure for determining changes in cellular proliferation, we studied the uptake of the thymidine analogue FLT. In contrast to the rapid decrease of FDG accumulation after the initiation of gefitinib treatment in H3255 cells, no change was observed at 2 hours post-treatment (data not shown), and only a 25% difference was detected at 4 hours post-treatment ($P = 0.11$, Fig. 2B). A dramatic decrease ($\sim$90%) in FLT uptake in H3255 cells was observed at day 2 of treatment ($P < 0.01$, Fig. 2B). In A549 cells, there were no significant changes in FLT uptake after treatment with 0.2 μmol/L of gefitinib ($P = 0.45$).

Both H3255 and A549 cells have a basal level of apoptosis of 7% to 8% Annexin V–positive cells (Fig. 2C). Treatment of H3255 cells with 0.2 μmol/L of gefitinib for 2 days caused an almost 2-fold increase in the fraction of Annexin V–positive cells (to 14.7 $\pm$ 0.3%; $P < 0.01$). There was no measurable increase in the number of apoptotic cells after 4 hours of gefitinib treatment ($P = 0.53$, Fig. 2C). Treatment of A549 cells with 0.2 μmol/L of gefitinib did not significantly increase the fraction of Annexin V–positive cells at either 4 hours or 2 days ($P = 0.45$, Fig. 2C).

Mechanism behind the effect of gefitinib on FDG uptake. FDG is transported into cells by the sodium-independent glucose transporter proteins (GLUT), then phosphorylated by hexokinase and thus trapped intracellularly. Treatment of H3255 cells with 0.2 μmol/L of gefitinib for 2 hours led to a slight $\sim$20% decrease of hexokinase activity in whole cell and mitochondria extracts ($P = 0.03$ and $P = 0.01$, respectively; Fig. 3A and B).

We next examined whether GLUT protein levels and function were affected by EGFR kinase inhibition. We investigated the functionality of GLUT transporters in gefitinib-treated H3255 cells by determining the uptake rates of 3-OMeG. 3-OMeG is a glucose analogue which cannot be phosphorylated by hexokinase; hence, the initial transport rate of 3-OMeG is a measure of glucose transport activity only (24). Following treatment with 0.2 μmol/L of gefitinib for 2 hours, the 3-OMeG transport rate of H3255 cells decreased from 0.050 $\pm$ 0.015/s to 0.019 $\pm$ 0.001/s (Fig. 3C).

The levels of GLUT transporter proteins were determined by Western blotting for H3255 cells (Fig. 3D). H3255 cells express GLUT3 but not GLUT1 (data not shown). Treatment with 0.2 μmol/L of gefitinib for 2 hours did not significantly decrease GLUT3 levels in whole cell lysates (Fig. 3D). However, no GLUT3 was detectable in the plasma membrane fraction of treated H3255 cells, whereas a noticeable increase of GLUT3 was observed in the cytosol fraction after gefitinib treatment. This result suggests that gefitinib causes the transporter to translocate from the plasma membrane to the cytosol.

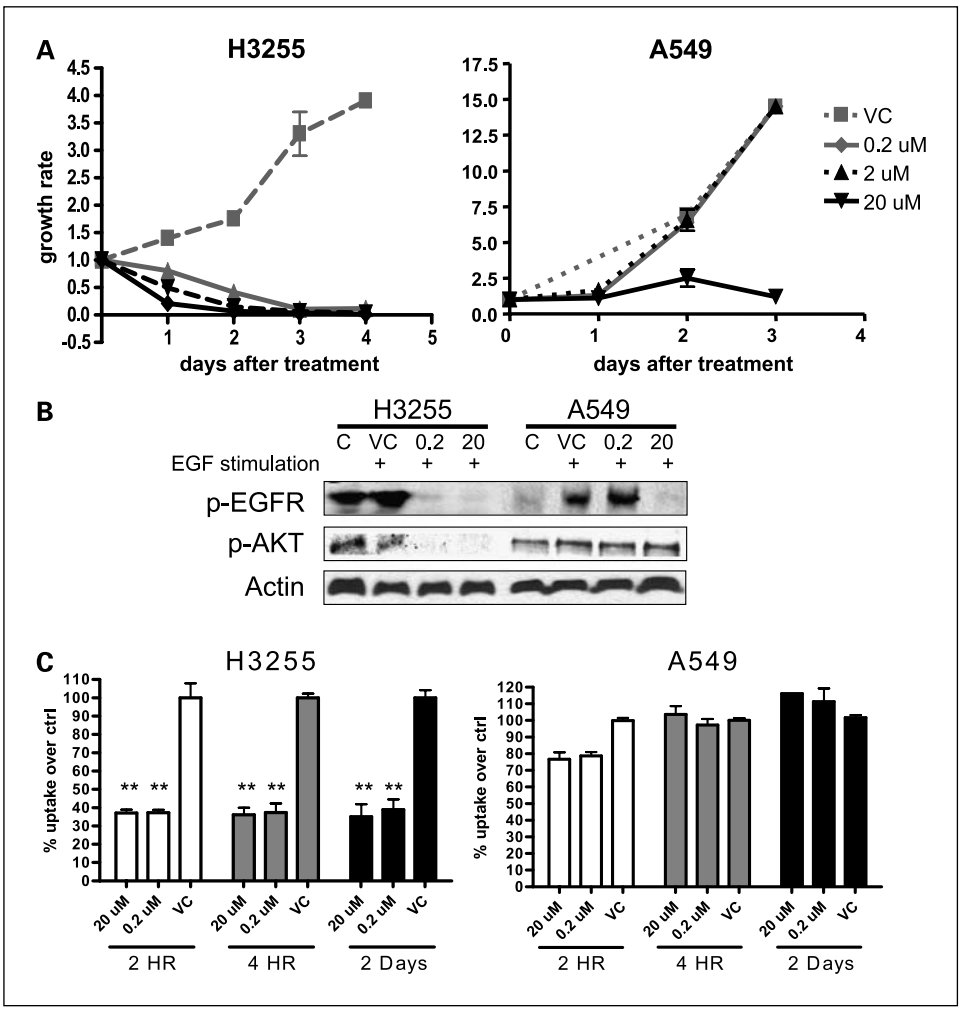

Fig. 1. Gefitinib sensitivity and FDG uptake of human tumor cell lines H3255 and A549. *A,* growth curves of cells treated with various amounts of gefitinib. *B,* Western blots of cell lysates. Cells were serum-starved, then treated with gefitinib for 4 hours, followed by epidermal growth factor stimulation. Two concentrations of gefitinib were used: 0.2 μmol/L (*0.2*) or 20 μmol/L (*20*). Vehicle control – treated cells (*VC*); control cells (*C*), which are untreated and unstimulated. *C,* FDG uptake for cells treated with gefitinib. Cells were treated with the indicated concentrations of gefitinib for the indicated times, then cellular FDG accumulation levels were determined after 1 hour of incubation with the radioactive probe. Uptake values are shown as radioactivity accumulation relative to vehicle-treated cells (*VC*). Bars, 1 SE. **, $P < 0.01$ for comparison with vehicle-treated controls (Bonferroni *post hoc* test).

Effect of gefitinib on FDG uptake of other cell lines. To determine whether our findings in H3255 and A549 cells may be generalized, we studied cell lines with other mechanisms for gefitinib sensitivity or resistance (Table 1). A gefitinib concentration of 1 μmol/L was used as the cutoff for sensitivity, as described in previous reports (29, 30). In the two sensitive cell lines, HCC4006 and A431, treatment with gefitinib caused inhibition of phospho-EGFR and phospho-AKT, although this effect was not quite as pronounced as in H3255 cells. Gefitinib had no effect on phospho-AKT and phospho-EGFR levels of the resistant cell line, H1975 (Fig. 4A). In HCC4006, FDG uptake decreased as rapidly, but not as pronounced as in H3255 cells ($P < 0.01$, Fig. 4B). In A431 cells, the reduction of FDG uptake after 2 hours of gefitinib treatment was only moderate ($P = 0.11$ and $P = 0.01$ for treatment with 0.2 and 20 μmol/L gefitinib, respectively). However, following 2 days of gefitinib treatment, the reduction of FDG uptake was comparable to H3255 cells ($P < 0.01$, Fig. 4C). In contrast, gefitinib did not cause a measurable decrease in FDG uptake in H1975 cells ($P > 0.9$, Fig. 4D).

Utilizing FDG PET imaging to monitor response to gefitinib treatment in mice. To determine whether the rapid decrease of FDG uptake in gefitinib-sensitive cells could be detected *in vivo* by FDG-PET, we imaged mice bearing xenografts of sensitive and resistant cell lines before and after treatment with gefitinib. In sensitive cell lines, there were dramatic reductions in FDG uptake after 2 days of gefitinib therapy, whereas no significant decreases of FDG uptake were observed in the resistant tumors, A549 (Fig. 5A) and H1975 (data not shown). Quantitative tumor FDG uptake decreased by at least 40% in all the gefitinib-sensitive cell lines ($P < 0.05$). In contrast, there were no measurable reductions of FDG uptake in the resistant cell lines (Fig. 5B).

Discussion

This study shows that, in gefitinib-sensitive cancer cells, EGFR kinase inhibition results in a rapid reduction of exogenous glucose utilization. This includes cells with EGFR kinase mutations (L858R or exon 19 deletions), as well as cells with amplification of wild-type EGFR. The effect of gefitinib on tumor metabolism preceded measurable changes in S phase fraction, thymidine uptake, and Annexin V binding. In contrast, gefitinib did not affect FDG uptake in resistant cell lines. Using PET imaging, sensitive and resistant tumors could be differentiated in tumor-bearing mice after only 2 days, following two oral doses of gefitinib. These findings make FDG-PET a very promising technique to predict tumor response to EGFR kinase early in the course of therapy.

Several patient characteristics, such as a history of not smoking, female gender, East Asian origin, and adenocarcinoma histology, are significantly associated with a greater benefit from treatment with EGFR kinase inhibitors (1–3, 31). More recently, specific mutations of the EGFR kinase domain have been shown to confer tumor sensitivity to treatment with gefitinib and erlotinib (6–8). However, as the number of patients with NSCLC undergoing EGFR mutation analysis has increased (31–33), it has become apparent that some tumors with mutations do not respond to treatment with EGFR kinase inhibitors. Conversely, a sizable subset of tumors, which do respond to gefitinib or erlotinib, seem to express only wild-type EGFR. Thus far, the reported positive and negative predictive values of EGFR kinase mutations for tumor response have varied widely (6–8, 31–33). This may be due to the fact that accurate evaluation of EGFR mutational status in clinical samples remains technically challenging and still needs to be standardized (4). In addition, several factors have been identified in experimental or clinical studies that can modulate the sensitivity of cancer cells to gefitinib. These include EGFR amplifications, overexpression of EGFR ligands (34), ErbB-3, and PTEN status (29, 35), secondary mutations of the EGFR kinase (16, 36), as well as the efflux of gefitinib mediated by multidrug transporters (37). Given the complexity of the ErbB signaling pathway and its well-documented cross-talk with other pathways (38), it will be challenging to develop a

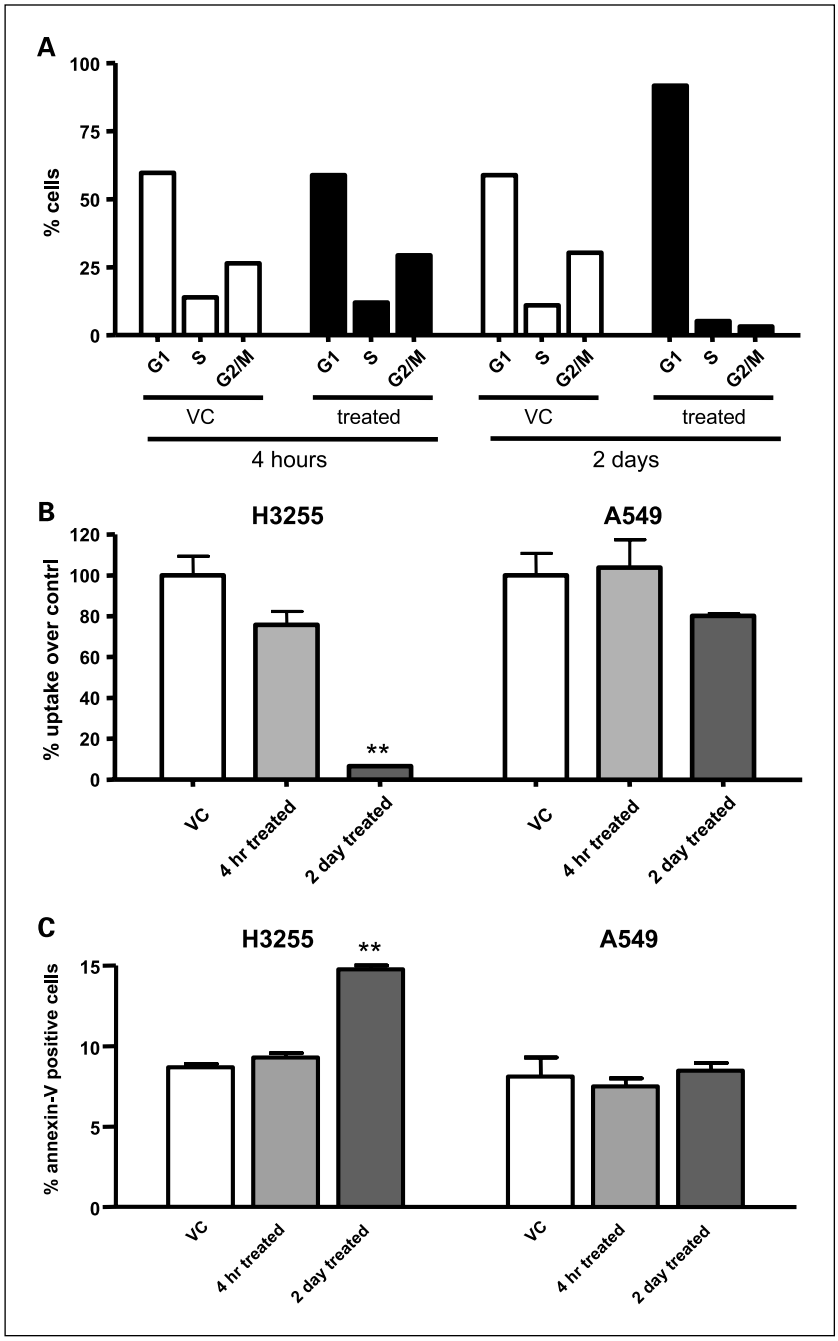

Fig. 2. Cell cycle analysis, FLT uptake, and apoptosis analysis of gefitinib-treated cells. Cells were treated with 0.2 μmol/L of gefitinib or vehicle for the indicated times. Vehicle control cells (*VC*). Bars, 1 SE. *A,* cell cycle analysis of H3255 cells. *B,* FLT uptake of H3255 and A549 cells. Uptake values are shown as radioactivity accumulation relative to vehicle-treated control cells. *C,* cells were treated with gefitinib and harvested for apoptosis analysis. Columns, mean percentage of cells that stained positive with Annexin V. **, $P < 0.01$ for comparison with vehicle-treated controls (Bonferroni *post hoc* tests).

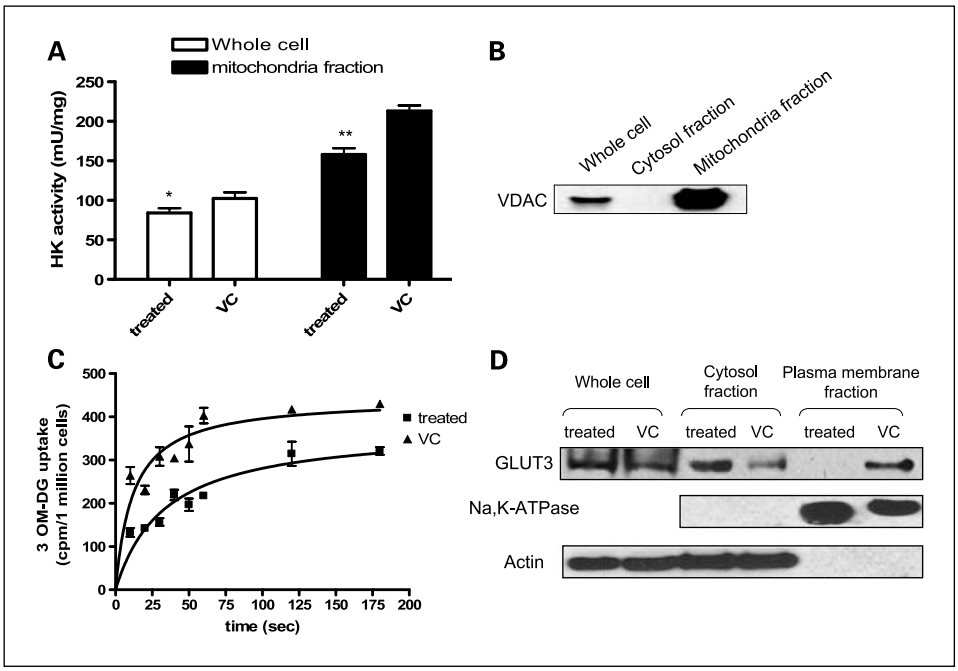

Fig. 3. Effect of gefitinib on hexokinase and glucose transporters. H3255 cells were treated with 0.2 μmol/L of gefitinib or vehicle for 2 hours. Vehicle control – treated cells (*VC*). Bars, 1 SE. *A,* hexokinase activity in whole cell extracts and mitochondrial fractions. Hexokinase activity was normalized to cellular protein content, and is represented as mU/mg. *B,* Western blot analysis of the mitochondria marker, VDAC, in various H3255 cellular fractions to confirm fraction purity. *C,* 3-OMeG transport in H3255 cells in response to gefitinib. Uptake values are presented as radioactivity (in cpm) per million viable cells. *D,* Western blot analysis of GLUT3, Na^+, K^+-ATPase, and actin levels in whole cells and cell membrane fractions of gefitinib-treated and vehicle-treated H3255 cells. Na^+, K^+-ATPase and actin levels were assessed to confirm fraction purity and also as loading controls. *, $P < 0.05$; **, $P < 0.01$ for comparison with vehicle-treated controls (unpaired *t* test).

complete model that takes into account all possible confounding factors for predicting the outcome of therapy in an individual patient.

For the reasons outlined above, we investigated an alternative approach to predict tumor response to the EGFR tyrosine kinase inhibitor gefitinib, by measuring early changes in tumor glucose use. Our cell culture data show that, in gefitinib-sensitive cell lines, FDG uptake per viable (trypan blue–negative) tumor cell decreases as early as 2 hours after exposure to the drug. These data suggest that the decrease of the FDG signal is not caused by cell death, but reflects changes in glucose metabolic activity of viable tumor cells. This suggestion is further supported by the observation that FDG uptake significantly decreases at a point in time when there is no increase in the fraction of Annexin V–positive cells. Furthermore, gefitinib-resistant cell lines did not show a measurable decrease in FDG uptake, even at the high, clinically irrelevant concentration of 20 μmol/L (30), which inhibited cell growth in culture after prolonged exposure.

Our data suggests that in sensitive cell lines, gefitinib leads to the translocation of glucose transporters from the plasma membrane to the cytosol, as shown by Western blots of the whole cell, cytosol, and plasma membrane fractions. The functional consequences of this translocation were confirmed

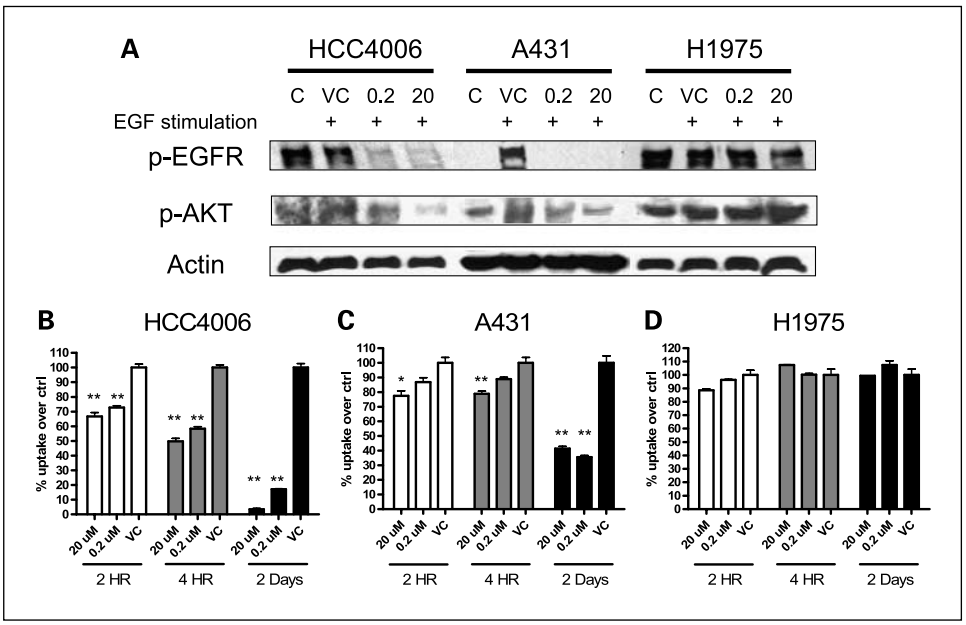

Fig. 4. Inhibition of EGFR signaling by gefitinib and its effect on FDG uptake in HCC4006, A431, and H1975 cells. *A,* Western blots of phospho-EGFR and phospho-AKT in response to gefitinib. Cells were serum-starved, then treated with gefitinib for 4 hours, followed by epidermal growth factor stimulation. Two concentrations of gefitinib were used: 0.2 μmol/L (*0.2*) or 20 μmol/L (*20*). Vehicle control – treated cells (*VC*); controls (*C*), which are untreated and unstimulated. *B-D,* FDG uptake of cells treated with gefitinib. Cells were treated with the indicated concentrations of gefitinib for the indicated times, then cellular FDG accumulation levels were determined 1 hour after incubation with the radioactive probe. Uptake values are represented as radioactivity accumulation relative to vehicle-treated cells (*VC*). Bars, 1 SE. *, $P < 0.05$; **, $P < 0.01$ for comparison with vehicle-treated controls (Bonferroni *post hoc* test).

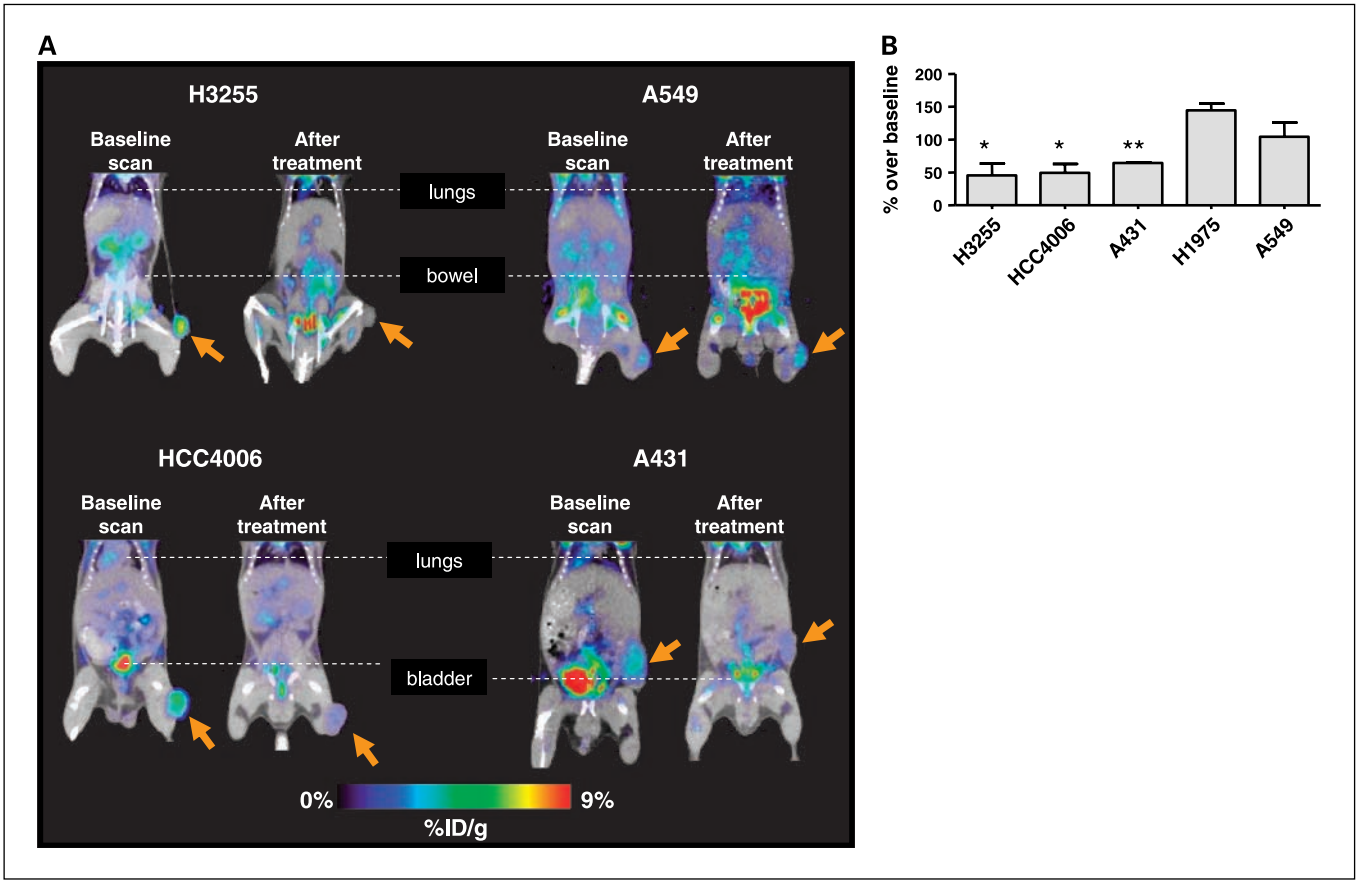

Fig. 5. MicroPET/CT imaging of human tumor xenografts before and after gefitinib treatment. *A,* tumor-bearing mice were subjected to a microPET/CT scan before (*Baseline scans*) and after two oral doses of gefitinib (70 mg/kg/d). Arrows, the locations of the tumors. *B,* quantitative analysis of changes in tumor FDG uptake in tumor xenografts. Columns, results from groups of at least three mice for each xenografted cell line; bars, 1 SE. *, $P < 0.05$; **, $P < 0.01$ for comparison of pretreatment and posttreatment scans (paired *t* test).

by determining glucose transport capacity with the metabolically stable glucose analogue, 3-OMeG. We observed a ~50% decrease of initial transport rates, and a ~25% decrease of uptake at equilibrium.

The second step of FDG metabolism, phosphorylation by hexokinase, was only modestly affected in whole cell and mitochondria extracts. However, we cannot rule out the significance of reduced glucose phosphorylation contributing to the rapid decrease of FDG uptake in sensitive cells. Hexokinase activity (39) was measured in cell extracts, which might not necessarily be representative for intact cells because complex biochemical interactions across the glycolytic and other related pathways can affect glucose phosphorylation rates. Further kinetic studies will be needed to determine which mechanism (or both) is the main factor in leading to the robust reduction of FDG accumulation in response to gefitinib.

Future studies are also needed to determine how the inhibition of EGFR signaling by gefitinib causes glucose transporter translocation and a consequent reduction in glucose uptake in sensitive cell lines. One possible mechanism could be through AKT, which is linked to glucose metabolism both in normal tissues and in cancer cells (40). Treatment with EGFR kinase inhibitors has been previously shown to inhibit AKT phosphorylation in gefitinib-sensitive, but not gefitinib-resistant tumors (19, 29, 41); which we confirmed in our study (Figs. 1B and 4A). We also observed a correlation between AKT inhibition and FDG uptake within the three sensitive cell lines. Compared with H3255 cells, A431 and HCC4006 cells showed less dramatic changes in FDG uptake and a less pronounced inhibition of AKT-phosphorylation in response to gefitinib.

Recent studies (42, 43) have shown that inhibition of two other protein kinases (c-kit and Bcr-Abl) with imatinib also induces a rapid loss of glucose transporters at the plasma membrane and decreases glucose transport rates. Taken together with our data, this suggests that there may be a close link between several oncogenic signaling proteins and glucose transport.

Although the results of our study support the idea that FDG-PET will be useful for predicting tumor response to EGFR kinase inhibitors in clinical trials, several limitations should be noted. First, we investigated the two best established mechanisms for sensitivity to EGFR kinase inhibitors (gene amplification and EGFR kinase domain mutations). However, other mechanisms may be clinically relevant, and it remains to be determined whether they are also associated with early changes in glucose metabolic activity during gefitinib treatment. Furthermore, the composition of human tumors is much more heterogeneous than that of mouse xenografts; hence, the reduction of FDG uptake in patients might not be as dramatic as in the mouse model system. However, clinical studies have shown that FDG

uptake of human tumors can be measured by FDG-PET with high reproducibility (11). Therefore, a treatment-induced reduction of FDG uptake in tumors in response to gefitinib may well be measurable in clinical studies, even if the changes are not as dramatic as in animal models.

In conclusion, our data provide a strong rationale to evaluate FDG-PET for the prediction of tumor response to EGFR kinase inhibitors in clinical trials. If these trials confirm the predictive value of metabolic changes for tumor response, FDG-PET in combination with molecular analysis of the tumor tissue may significantly reduce the side effects (44) and costs of ineffective therapy. In preclinical models, several irreversible EGFR kinase inhibitors have been shown to be effective in cancer cells that are resistant to gefitinib and erlotinib (45, 46). Therefore, rapid, noninvasive imaging techniques to monitor tumor responses are likely to become even more important in the future because treatment may be adjusted in patients with primary or secondary resistance to gefitinib or erlotinib.

Acknowledgments

We thank Dr. Bruce Johnson for providing H3255 cells and Drs. John Minna and Michael Peyton for providing HCC4006 cells. We thank Waldemar Ladno, Judy Edwards, Victor Dominguez, and Dr. David Stout for excellent animal imaging technical assistance and the UCLA Cyclotron staff for providing the radiolabeled compounds. We thank Dr. Jing Huang for allowing us to use the UV-Visible Spectrophotometer 8453. Flow cytometry was done in the UCLA Jonsson Comprehensive Cancer Center and Center for AIDS Research Flow Cytometry Core Facility that is supported by NIH awards CA-16042 and AI-28697, and by the Jonsson Comprehensive Cancer Center, the UCLA AIDS Institute, and the David Geffen School of Medicine at UCLA.

References

1. Kris MG, Natale RB, Herbst RS, et al. Efficacy of gefitinib, an inhibitor of the epidermal growth factor receptor tyrosine kinase, in symptomatic patients with non-small cell lung cancer: a randomized trial. JAMA 2003;290:2149–58.
2. Fukuoka M, Yano S, Giaccone G, et al. Multi-institutional randomized phase II trial of gefitinib for previously treated patients with advanced non-small-cell lung cancer (The IDEAL 1 Trial) [corrected]. J Clin Oncol 2003;21:2237–46.
3. Shepherd FA, Rodrigues Pereira J, Ciuleanu T, et al. Erlotinib in previously treated non-small-cell lung cancer. N Engl J Med 2005;353:123–32.
4. Giaccone G, Rodriguez JA. EGFR inhibitors: what have we learned from the treatment of lung cancer? Nat Clin Pract Oncol 2005;2:554–61.
5. Pao W, Miller VA. Epidermal growth factor receptor mutations, small-molecule kinase inhibitors, and non-small-cell lung cancer: current knowledge and future directions. J Clin Oncol 2005;23:2556–68.
6. Paez JG, Janne PA, Lee JC, et al. EGFR mutations in lung cancer: correlation with clinical response to gefitinib therapy. Science 2004;304:1497–500.
7. Lynch TJ, Bell DW, Sordella R, et al. Activating mutations in the epidermal growth factor receptor underlying responsiveness of non-small-cell lung cancer to gefitinib. N Engl J Med 2004;350:2129–39.
8. Pao W, Miller V, Zakowski M, et al. EGF receptor gene mutations are common in lung cancers from "never smokers" and are associated with sensitivity of tumors to gefitinib and erlotinib. Proc Natl Acad Sci U S A 2004;101:13306–11.
9. Weber WA, Petersen V, Schmidt B, et al. Positron emission tomography in non-small-cell lung cancer: prediction of response to chemotherapy by quantitative assessment of glucose use. J Clin Oncol 2003;21:2651–7.
10. Hoekstra CJ, Stroobants SG, Smit EF, et al. Prognostic relevance of response evaluation using [18F]-2-fluoro-2-deoxy-D-glucose positron emission tomography in patients with locally advanced non-small-cell lung cancer. J Clin Oncol 2005;23:8362–70.
11. Weber WA. Use of PET for monitoring cancer therapy and for predicting outcome. J Nucl Med 2005;46:983–95.
12. Stroobants S, Goeminne J, Seegers M, et al. 18FDG-Positron emission tomography for the early prediction of response in advanced soft tissue sarcoma treated with imatinib mesylate (Glivec). Eur J Cancer 2003;39:2012–20.
13. Demetri GD, von Mehren M, Blanke CD, et al. Efficacy and safety of imatinib mesylate in advanced gastrointestinal stromal tumors. N Engl J Med 2002;347:472–80.
14. Merlino GT, Xu YH, Ishii S, et al. Amplification and enhanced expression of the epidermal growth factor receptor gene in A431 human carcinoma cells. Science 1984;224:417–9.
15. Janmaat ML, Rodriguez JA, Gallegos-Ruiz M, Kruyt FA, Giaccone G. Enhanced cytotoxicity induced by gefitinib and specific inhibitors of the Ras or phosphatidyl inositol-3 kinase pathways in non-small cell lung cancer cells. Int J Cancer 2006;118:209–14.
16. Pao W, Miller VA, Politi KA, et al. Acquired resistance of lung adenocarcinomas to gefitinib or erlotinib is associated with a second mutation in the EGFR kinase domain. PLoS Med 2005;2:e73.
17. Peyton M, Girard L, Shigematsu H, et al. Gefitinib and erlotinib sensitivity in a panel of non-small cell lung cancer (NSCLC) cell lines [abstract #3389]. Proc Amer Assoc Cancer Res 2005;46.
18. Seimbille Y PM, Czernin J, Silverman DH. Fluorine-18 labeling of 6,7-disubstituted anilinoquinazoline derivatives for positron emission tomography (PET) imaging of tyrosine kinase receptors: synthesis of 18F-Iressa and related molecular probes. J Labelled Comp Radiopharm 2005;48:829–43.
19. Amann J, Kalyankrishna S, Massion PP, et al. Aberrant epidermal growth factor receptor signaling and enhanced sensitivity to EGFR inhibitors in lung cancer. Cancer Res 2005;65:226–35.
20. Waldherr C, Mellinghoff IK, Tran C, et al. Monitoring antiproliferative responses to kinase inhibitor therapy in mice with 3′-deoxy-3′-18F-fluorothymidine PET. J Nucl Med 2005;46:114–20.
21. Yu WH, Forte M. Is there VDAC in cell compartments other than the mitochondria? J Bioenerg Biomembr 1996;28:93–100.
22. Gottardi CJ, Caplan MJ. Molecular requirements for the cell-surface expression of multisubunit ion-transporting ATPases. Identification of protein domains that participate in Na,K-ATPase and H,K-ATPase subunit assembly. J Biol Chem 1993;268:14342–7.
23. Robey RB, Raval BJ, Ma J, Santos AV. Thrombin is a novel regulator of hexokinase activity in mesangial cells. Kidney Int 2000;57:2308–18.
24. Aloj L, Caraco C, Jagoda E, Eckelman WC, Neumann RD. Glut-1 and hexokinase expression: relationship with 2-fluoro-2-deoxy-D-glucose uptake in A431 and T47D cells in culture. Cancer Res 1999;59:4709–14.
25. Tai YC, Ruangma A, Rowland D, et al. Performance evaluation of the microPET focus: a third-generation microPET scanner dedicated to animal imaging. J Nucl Med 2005;46:455–63.
26. Chow P, Stout D, Komisopoulou E, Chatziioannou A. A method of image registration for small animal, multi-modality imaging. Phys Med Biol 2005;51:379–90.
27. Loening AM, Gambhir SS. AMIDE: a free software tool for multimodality medical image analysis. Mol Imaging 2003;2:131–7.
28. Green LA, Gambhir SS, Srinivasan A, et al. Noninvasive methods for quantitating blood time-activity curves from mouse PET images obtained with fluorine-18-fluorodeoxyglucose. J Nucl Med 1998;39:729–34.
29. Engelman JA, Janne PA, Mermel C, et al. ErbB-3 mediates phosphoinositide 3-kinase activity in gefitinib-sensitive non-small cell lung cancer cell lines. Proc Natl Acad Sci U S A 2005;102:3788–93.
30. Baselga J, Rischin D, Ranson M, et al. Phase I safety, pharmacokinetic, and pharmacodynamic trial of ZD1839, a selective oral epidermal growth factor receptor tyrosine kinase inhibitor, in patients with five selected solid tumor types. J Clin Oncol 2002;20:4292–302.
31. Tsao MS, Sakurada A, Cutz JC, et al. Erlotinib in lung cancer—molecular and clinical predictors of outcome. N Engl J Med 2005;353:133–44.
32. Han SW, Kim TY, Hwang PG, et al. Predictive and prognostic impact of epidermal growth factor receptor mutation in non-small-cell lung cancer patients treated with gefitinib. J Clin Oncol 2005;23:2493–501.
33. Cappuzzo F, Hirsch FR, Rossi E, et al. Epidermal growth factor receptor gene and protein and gefitinib sensitivity in non-small-cell lung cancer. J Natl Cancer Inst 2005;97:643–55.
34. Ishikawa N, Daigo Y, Takano A, et al. Increases of amphiregulin and transforming growth factor-α in serum as predictors of poor response to gefitinib among patients with advanced non-small cell lung cancers. Cancer Res 2005;65:9176–84.
35. Bianco R, Shin I, Ritter CA, et al. Loss of PTEN/MMAC1/TEP in EGF receptor-expressing tumor cells counteracts the antitumor action of EGFR tyrosine kinase inhibitors. Oncogene 2003;22:2812–22.
36. Kobayashi S, Ji H, Yuza Y, et al. An alternative inhibitor overcomes resistance caused by a mutation of the epidermal growth factor receptor. Cancer Res 2005;65:7096–101.
37. Elkind NB, Szentpetery Z, Apati A, et al. Multidrug transporter ABCG2 prevents tumor cell death induced by the epidermal growth factor receptor inhibitor Iressa (ZD1839, Gefitinib). Cancer Res 2005;65:1770–7.
38. Mendelsohn J. Targeting the epidermal growth factor receptor for cancer therapy. J Clin Oncol 2002;20:1–13S.
39. Wilson JE. Isozymes of mammalian hexokinase: structure, subcellular localization and metabolic function. J Exp Biol 2003;206:2049–57.
40. Hajduch E, Litherland GJ, Hundal HS. Protein kinase

B (PKB/Akt)—a key regulator of glucose transport? FEBS Lett 2001;492:199–203.

41. Janmaat ML, Kruyt FA, Rodriguez JA, Giaccone G. Response to epidermal growth factor receptor inhibitors in non-small cell lung cancer cells: limited antiproliferative effects and absence of apoptosis associated with persistent activity of extracellular signal-regulated kinase or Akt kinase pathways. Clin Cancer Res 2003;9:2316–26.

42. Cullinane C, Dorow DS, Kansara M, et al. An *in vivo* tumor model exploiting metabolic response as a biomarker for targeted drug development. Cancer Res 2005;65:9633–6.

43. Barnes K, McIntosh E, Whetton AD, Daley GQ, Bentley J, Baldwin SA. Chronic myeloid leukaemia: an investigation into the role of Bcr-Abl-induced abnormalities in glucose transport regulation. Oncogene 2005;24:3257–67.

44. Takano T, Ohe Y, Kusumoto M, et al. Risk factors for interstitial lung disease and predictive factors for tumor response in patients with advanced non-small cell lung cancer treated with gefitinib. Lung Cancer 2004;45:93–104.

45. Carter TA, Wodicka LM, Shah NP, et al. Inhibition of drug-resistant mutants of ABL, KIT, and EGF receptor kinases. Proc Natl Acad Sci U S A 2005;102:11011–6.

46. Kwak EL, Sordella R, Bell DW, et al. Irreversible inhibitors of the EGF receptor may circumvent acquired resistance to gefitinib. Proc Natl Acad Sci U S A 2005;102:7665–70.

Clinical Cancer Research

Monitoring Tumor Glucose Utilization by Positron Emission Tomography for the Prediction of Treatment Response to Epidermal Growth Factor Receptor Kinase Inhibitors

Helen Su, Claudia Bodenstein, Rebecca A. Dumont, et al.

Clin Cancer Res 2006;12:5659-5667.